Journal of Power Sources 194 (2009) 550–557

Contents lists available at ScienceDirect

Journal of Power Sources

journal homepage: www.elsevier.com/locate/jpowsour

Analysis of internal short-circuit in a lithium ion cell

Shriram Santhanagopalan*, Premanand Ramadass, John (Zhengming) Zhang

Celgard LLC, 13800 South Lakes Drive, Charlotte, NC 28273, United States

ARTICLE INFO

Article history:
Received 16 March 2009
Received in revised form 30 April 2009
Accepted 1 May 2009
Available online 12 May 2009

Keywords:
Lithium ion cell
Internal short-circuit
Mathematical model

ABSTRACT

An electrochemical thermal model was developed to study the internal short-circuit behavior of a lithium ion cell. The model was used to understand several experimental observations: several short-circuit scenarios possible in a lithium ion cell were simulated and the power generated from each case was calculated. Influence of parameters like the SOC and initial temperature of the cell was studied.

Experiments were carried out to verify the predictions made using the model. Some pointers are provided towards design of a safer cell.

1. Introduction

Safety has been the primary issue in the use of the lithium ion technology in high energy and high power applications ranging from power tools to electric vehicles. The increasing demand for energy and the rise in the number of field incidents associated with commercial lithium ion cells have forced investigators and the industries alike, to study the behavior of the lithium ion cell under abuse conditions. Spotnitz and Franklin [1] provide an excellent summary of the various chemical reactions that characterize the abuse behavior of high power lithium ion cells. Experimental investigation of the thermal runaway reactions have been extensively carried out by Dahn et al. [2] and Botte et al. [3] measured the stability of different electrolytes using DSC measurements. Onda et al. [4] measured the heat generation rate as a function of the state of charge of the cell. Roth et al. [5] investigated the contributions from different electrolytes as well as several cathode materials experimentally using calorimetric measurements. Yamauchi et al. [6] studied the internal short-circuit behavior. Hatchard et al. [2] developed a heat transfer model that considers joule heating of the cell during a thermal runaway. Empirical correlations were developed for dependence of the parameters on temperature. A similar model that includes heat generated from chemical reactions was proposed by Kim et al. [7] for a more sophisticated geometry. The rates for the chemical reactions were modeled as functions of temperature and Arrhenius type relationships were used. The activation energies for the individual reactions were simulated as functions of the temperature. Spotnitz et al. [8] extended Hatchard's model [2] to three dimensions and demonstrated the heat dissipation properties in cells of different sizes. Abraham et al. [9] studied these reactions within an 18650 type cell using accelerated rate calorimetry. Similar investigations were undertaken by Barnett et al. [10] Other efforts towards understanding the behavior of the battery have focused on thermal-electrochemical models under regular operating conditions of the cell.

In the present work, we illustrate the utility of a thermal-electrochemical model in predicting the behavior of a lithium ion cell during an internal short-circuit. The model includes the distributions of the various abuse reactions as well as temperature within the cell. Several case studies are shown, to better understand the phenomenon of internal short-circuit in the light of cell safety. Coupling the electrochemical model with the thermal response provides for a more realistic heat propagation mechanism compared to an isolated thermal model, since localized reactions are now treated as functions of the electrochemical states. A typical need for such a model arises when one investigates parameters like the critical area of short-circuit beyond which the runaway process will initiate, for a cell of pre-specified dimensions and capacity. The rigorous model presented here can identify differences in the thermal response of the cell as shown in a later section, between a micro-short, for example due to a lithium dendrite, that can easily burn out due to the heat generated and a persistent short, for example due to metal contamination, that will lead to a runaway. The behavior of the cell under a variety of such practical scenario is studied using the model and some predictions are verified by experimental studies.

2. Model development

There are two parts in the battery model described here. The first part of the model describes the behavior of the cell under normal

* Corresponding author at: Celgard LLC, 13800 South Lakes Drive, Charlotte, NC 28273, United States.
E-mail address: shriramsanthanagopalan@celgard.com (S. Santhanagopalan).

0378-7753/$ – see front matter © 2009 Elsevier B.V. All rights reserved.
doi:10.1016/j.jpowsour.2009.05.002

Nomenclature

List of symbols

a_i	specific surface area ($m^2\ m^{-3}$)
c_p	specific heat capacity ($J\ kg^{-1}\ K^{-1}$)
c_j	concentration of species j ($mol\ m^{-3}$)
$\dot{c}_{k,j}$	rate of change of concentration of species j taking part in reaction k.
D	diffusion coefficient ($m^2\ s^{-1}$)
E_{act}	energy of activation ($J\ mol^{-1}$)
F	Faraday's constant ($C\ mol^{-1}$)
H_j	heat of reaction for reactant j ($J\ kg^{-1}$)
i_{short}	short-circuit current ($A\ m^{-2}$)
$j_{n,i}$	rate of electrochemical reaction ($mol\ m^{-2}\ s^{-1}$)
M_k	molecular weight of reaction k ($kg\ mol^{-1}$)
$P_{k,j}$	order of the reaction j with respect to reactant k
q	rate of heat generation ($W\ m^{-3}$)
R_j	rate of reaction j ($mol\ m^{-3}\ s^{-1}$)
R	gas constant ($8.314\ J\ mol^{-1}\ K^{-1}$)
K_j	rate constant for reaction j ($(mol\ m^{-3})^{1-p_{k,j}}\ s^{-1}$)
t	time (s)
T	temperature (K)
U_i	open circuit potential (V)

Greek and latin

κ_{eff}	effective electrical conductivity of lithium ions in the electrolyte ($\Omega^{-1}\ m^{-1}$)
λ	thermal conductivity ($W\ m^{-1}\ K^{-1}$)
Φ_k	potential within phase k (V)
ρ	density ($kg\ m^{-3}$)
φ	temperature dependent property (see Eq. (5))
σ_{eff}	effective electrical conductivity of lithium ions in the electrode ($\Omega^{-1}\ m^{-1}$)

operating conditions based on the porous electrode framework [11]. These equations describe the change in the potential and concentration of lithium within each electrode and inside the electrolyte as functions of time and position. The limitations from the transport within both the solid and solution phase are accounted for as are any kinetic limitations as a result of the ion transfer at the interface of the electrodes and the electrolyte. These equations are well documented in the literature [12–15] and are hence not reproduced here for brevity.

The second part of the model describes the framework to monitor the rise in the cell temperature. The generalized energy balance equation is given by [13]:

$$\frac{\partial(\rho c_p T)}{\partial t} = \nabla \cdot \lambda \nabla T + q \tag{1}$$

where ρ is the density, c_p is the heat capacity and λ is the thermal conductivity. Note that these are volume averaged parameters for the respective components; for example, within the anode, the density is volume averaged to include the properties of the active material, binder and fillers. The term q is associated with heat generated from various sources such as joule heating, electrochemical reactions that take place during the normal operating conditions and chemical reactions during a thermal runaway. The heat generated from the thermal runaway reactions is included inside the source term q as follows:

$$q = a_i F j_{n,i} \left(\Phi_1 - \Phi_2 - U_i + T \frac{\partial U_i}{\partial T} \right) + \sigma_{eff,i} \nabla \Phi_1 \cdot \nabla \Phi_1 + \kappa_{eff,i} \nabla \Phi_2 \cdot \nabla \Phi_2 + \sum_j \sum_k \dot{c}_{k,j} M_k H_j \tag{2}$$

where $c_{k,j}$ are concentrations of the individual components (k) of the cell taking part in the runaway reactions (j), M_k is the molecular weight of component k and H_j is the heat of reaction for the thermal runaway reaction j. Note that H_j for individual components can be obtained using DSC measurements [1]. The change in the composition of the electrodes is tracked using material balances for the individual species (k), given by:

$$\dot{c}_{k,j} = \nabla \cdot (D_k \nabla c_{k,j}) + R_j \tag{3}$$

where the left hand side represents the rate of change in the concentration of component k with time, the first term on the right hand side includes transport limitations, if any and the second term R_j represents the chemical (or electrochemical) reactions causing decomposition of c_k in the reaction j. The chemical reaction terms are modeled using concentration dependent rate expressions of the following form:

$$R_j = K_j \prod_k c_{k,j}^{p_{k,j}} \tag{4}$$

Here the term K_j represents the rate constant for the reaction j and is a function of temperature as described by Eq. (5) below and $p_{k,j}$ represent the order of reaction j with respect to species k. The details for the individual material balances and parameters for the different reactions are described by Spotnitz et al. [1] In Eq. (3) the transport limitations are usually neglected since the time constants for the runaway reactions are several orders of magnitude smaller than those required for the transport limitations to set in. Thus, the last term on Eq. (2) represents the differential amount of heat generated, as a function of accessibility and reactivity of the different species k taking part in reactions j, as a function of position and time.

Important parameters like the ionic conductivity of the electrolyte and reaction rate constants are modeled as functions of temperature using Arrhenius type relationships:

$$\varphi = \varphi_{ref} \exp\left[\frac{E_{act,\varphi}}{R} \left(\frac{1}{T_{ref}} - \frac{1}{T} \right) \right] \tag{5}$$

where φ_{ref} refers to the property of interest at the reference temperature T_{ref} and $E_{act,\varphi}$ refers to the activation energy for the change in the property φ with temperature.

The short-circuit is assumed to be an instantaneous discrete process; i.e., at $t \geq t_{short}$ there appears an electrically continuous path between the two layers undergoing the short. Fig. 1 illustrates this idea. The flow of current through the short is described using Ohm's law:

$$i_{short} = -\sigma_{short} \nabla (\Phi_{1,i} - \Phi_{1,j}) \tag{6}$$

where σ_{short} is the conductivity of the short. The subscripts i and j refer to the two layers undergoing the shorts and $\phi_{1,i}$ and $\phi_{1,j}$ refer to the local solid phase potentials at the two layers respectively. Thus at $t \geq t_{short}$ the energy balance equation is represented by the following expression:

$$q = a_i F j_{n,i} \left(\Phi_1 - \Phi_2 - U_i + T \frac{\partial U_i}{\partial T} \right) + \sigma_{short} \nabla (\Phi_{1,i} - \Phi_{1,j}) \cdot \nabla (\Phi_{1,i} - \Phi_{1,j}) + \kappa_{eff,i} \nabla \Phi_2 \cdot \nabla \Phi_2 + \sum_j \sum_k \dot{c}_{k,j} M_k H_j \tag{7}$$

As described later, the conductivity of the short (σ_{short}) is determined as the minimum value of the two components undergoing the short. The transport of charge across the short takes place primarily across the solid phases of the participating components; since electronic transport is much faster compared to the movement of the ions across the solution, in practice, the ohmic term dominates the first few microseconds of the short, before the liquid phase migration and transport limitations within the solid phase

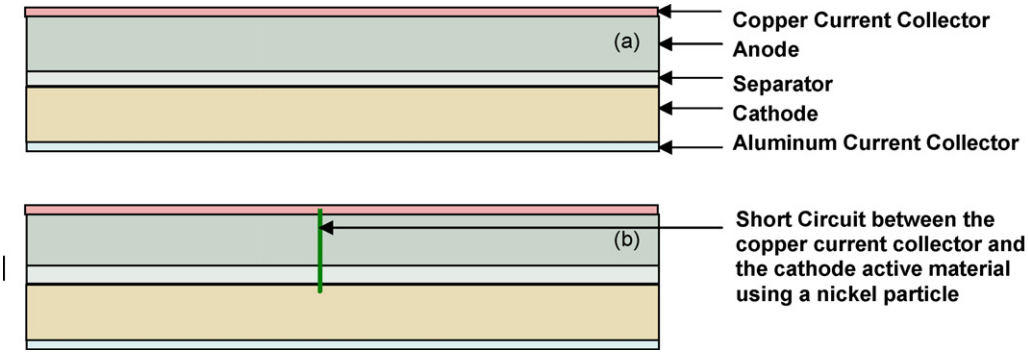

Fig. 1. Diagrammatic representation of an internal short-circuit: (a) the model of the cell under normal operating conditions (i.e., $t < t_{short}$); (b) the situation where the short between a current collector and the other electrode, due to the penetration of particles from the current collector.

take over; thus the Joule heating plays a key role in initiating the temperature rise at the point of short.

The introduction of the internal short expression to the energy balance results in a coupling of the electrochemical behavior with the thermal response of the cell during the short. Since the properties of the various components used are described as functions of temperature, the resultant rise in temperature from the source term q, which is initially just Joule heating, quickly leads to initiation of the abuse reactions at the corresponding temperatures. The last term on Eq. (7) includes the enthalpies of the different reactions and hence results in further increase in the value of heat generated. This chain of heat generation processes, under the right set of conditions lead to the thermal runaway during the internal short-circuit. The use of rigorous material balance for the individual species allows one to study the effect of the local chemistry of the cell (e.g., the SOC at the spot where the short originates) on the thermal behavior of the cell during a short-circuit. The next section describes in more detail the different cases possible during an internal short and provides a summary of the various parameters that determine the course of the runaway process.

3. Results and discussion

The model presented here is an extension of the porous electrode thermal-electrochemical model presented by Gu and Wang [13]. The cell design parameters and the properties of the materials are shown in Table 1. The energy balance (Eq. (1)) is modified to include the heat generated due to chemical reactions. The reaction rates are modeled as shown in the work by Kim et al. [7] The material and energy balance equations were solved simultaneously using a finite element based package called Comsol Multiphysics ©using a time dependent solver and adaptive time stepping. The relative tolerance was set to 1e−6 and the number of degrees of freedom was about 4,500,000. When required, the variables were scaled automatically by the solver.

A material balance for the individual components of the cell is shown in Eq. (3). There is a significant change in the concentration of the electrolyte during the short; however, the time constant for the runaway reactions is so small that the contribution from the diffusion term within the time-frame of several milliseconds is negligible and is hence ignored in these material balance equations. The reaction term on the material balance has a temperature dependent rate constant and the product of the reactants raised to suitable orders. The values for the parameters that appear in the abuse reactions were obtained from the work of Spotnitz et al. [1]. Fig. 2 shows the maximum contributions from the different components of the cell to the heat generated during the runaway process within the cell. In generating this figure, it was assumed that all components undergo complete reaction and/or combustion. As observed, the

Table 1
List of parameters used in the model[a].

Parameter	Value	Unit
Thickness of cathode ($LiCoO_2$)	65	μm
Thickness of anode (MCMB)	60	μm
Thickness of the separator	16	μm
Thickness of the current collectors	15	μm
Length of the electrode	32	cm
Width of the electrode	40	mm
Initial electrolyte concentration	1000	mol m^{-3}
Ambient temperature	298.15	K
Diffusion coefficient of Li^+ at the anode	3.9e−14	m^2 s^{-1}
Diffusion coefficient of Li^+ at the cathode	1.2e−13	m^2 s^{-1}
Particle size (diameter)	20	μm
Porosity of the electrode	0.15	–
Capacity of the cell	800	mAh
Electrical conductivity of the anode	100	S m^{-1}
Electrical conductivity of the cathode	3.8	S m^{-1}
Electrical conductivity of the anode current collector	6.0e5	S m^{-1}
Electrical conductivity of the anode current collector	3.8e5	S m^{-1}
Density of electrolyte	1324.0	kg m^{-3}
Density of negative material	1800.0	kg m^{-3}
Density of positive active material	4280.0	kg m^{-3}
Heat capacity of copper	381.0	J kg^{-1} K^{-1}
Heat capacity of anode	700.0	J kg^{-1} K^{-1}
Heat capacity of separator	1300.0	J kg^{-1} K^{-1}
Heat capacity of cathode	1100.0	J kg^{-1} K^{-1}
Heat capacity of aluminum	870.0	J kg^{-1} K^{-1}
Thermal conductivity of copper	380	W m^{-1} K^{-1}
Thermal conductivity of anode	5	W m^{-1} K^{-1}
Thermal conductivity of separator	1	W m^{-1} K^{-1}
Thermal conductivity of cathode	1.8	W m^{-1} K^{-1}
Thermal conductivity of aluminum	200	W m^{-1} K^{-1}

[a] All other parameters used were from Refs. [1] and [8].

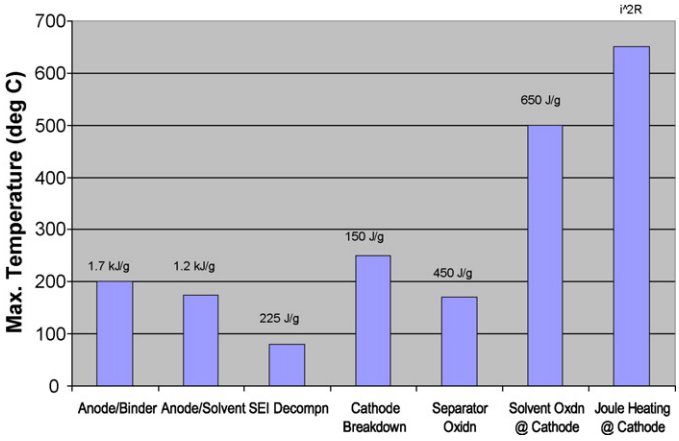

Fig. 2. Maximum rise in local temperature during a thermal runaway due to abuse reactions in which the various components of the cell take part: also shown are the heat generating capabilities assuming complete combustion of the various components.

contribution from the breakdown of the solid–electrolyte interface (SEI) layer, and that from the binder–solvent interactions are negligible. Similar results were also reported by Spotnitz et al. [1] The figure also shows the origin of the abuse reactions at the anode at a much lower temperature compared to those at the cathode, essentially implying the critical role played by the anode in raising the cell temperature to higher values, at which point the cathode decomposition and other reactions take over. These results are used in the following section to explain the behavior of a lithium ion cell, under different short-circuit scenarios. Although the results shown here are restricted to cell parameters shown in these tables, the observations are in general applicable to most commonly used lithium ion cells. In this sense, one must limit the numeric analysis of the results to the cases presented here, while realizing the generality of the predictions to a wide array of parameters.

3.1. Impact of the nature of short

In a lithium ion cell, four different short-circuit scenarios are probable: (i) the short between the two current collectors (copper and aluminum), (ii) the short between the copper current collector and the cathode active material, (iii) the short between the aluminum current collector and the anode material, and (iv) the short between the active materials on both the electrodes. The results for these short scenarios are discussed in the rest of this section. In any of the above cases, the electrical resistivity of the short is calculated as the maximum of the resistivity of the two elements associated with the short. In other words, the two elements that undergo the short are treated as resistances in series, and the current flow across the short-circuit is determined by the maximum resistance in the flow path. Thus, the conductivity of the (σ_{short}) is in essence, the minimum of the individual conductivity of the components involved in the short.

(i) *Copper/aluminum short*. This short-circuit scenario is quite similar to connecting a low resistance externally across the tabs of the cell. In general, the skin temperature of the cell during an external short-circuit rises to a maximum of about 100 °C before it starts to cool down. A similar scenario results during the internal short between the current collectors. Based on the arguments above, σ_{short} is equivalent to that of aluminum. As a result, the energy associated with the Type i short-circuit is the largest. Fig. 3 shows the increase in the power generated as predicted by the model for this case. As observed, there is an increase in power generated for the first few seconds, due to rapid flow of current across the Type i short. The rise in local temperature as a function of time is shown in Fig. 4. The temperature of the cell rises steadily for the first few seconds. However, copper and aluminum being extremely good conductors of heat, the localized heat accumulation around the short area is minimal. As a result, the temperature rise for this case is kept under check soon after the initial rise, and hence starts to decline. The rate of decline depends on the ambient temperature and the mode of cooling, to which the cell is subjected to.

(ii) *Copper/cathode active material short*. In most cells, by virtue of design, the short between the copper current collector and the cathode active material is fairly infrequent. For the Type ii short-circuit, the short resistance is controlled by the active material. Since the cathode mix is the poorest of conductors among the four components as shown in Table 1, the current flow for this case is minimal. Any rise in temperature is limited to the Joule heating (i.e., I^2R power loss) regime. The power liberated is usually not sufficient for the temperature to reach values at which the chemical reactions are triggered. Note that in Fig. 3, the heat generation rate is minimal for this case compared to the others.

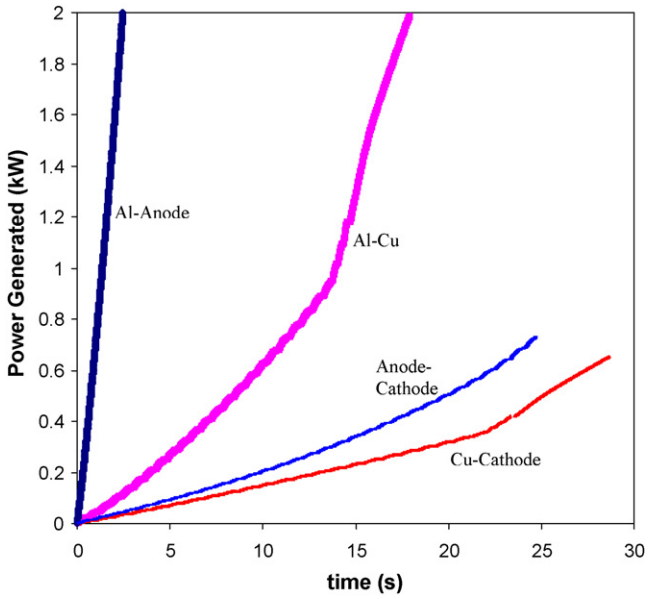

Fig. 3. Power generated after various types of short-circuit scenario in a lithium ion cell: Type i, short occurs between the two current collectors; Type ii, short occurs between copper current collector and the cathode active material; Type iii, short occurs between aluminum and the anode material; Type iv, short occurs between active material at the cathode and the anode.

(iii) *Aluminum/anode short*. In the case of short-circuit between metallic aluminum from the cathode current collector and the anode active material, there are two crucial factors that subscribe to the runaway behavior of the cell. The anode material has a very low electrical resistivity, leading to a high power short (almost at par with a Type i short) as shown in Fig. 3. At the same time, the onset temperatures for the reactions at the anode are low compared to those at the cathode. The third

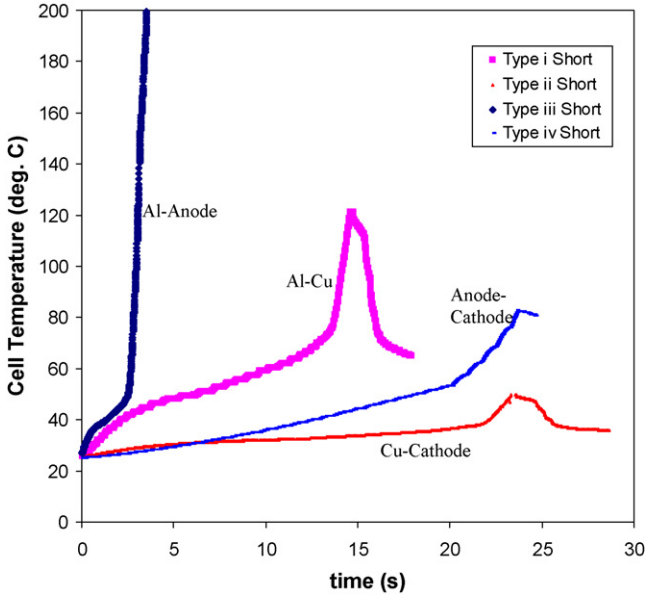

Fig. 4. Local temperature after various types of short-circuit scenario in a lithium ion cell: Type i, short occurs between the two current collectors; Type ii, short occurs between copper current collector and the cathode active material; Type iii, short occurs between aluminum and the anode material; Type iv, short occurs between active material at the cathode and the anode.

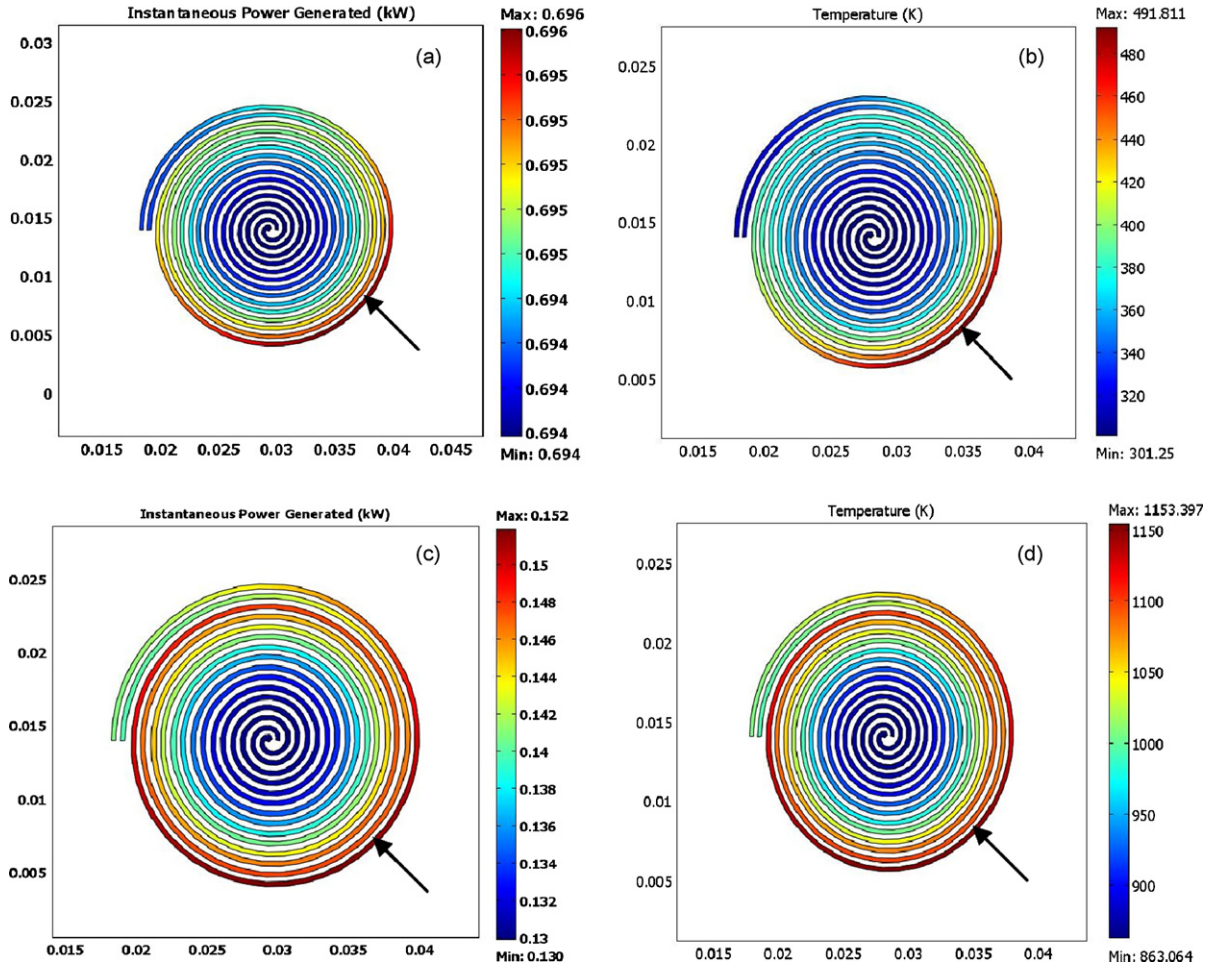

Fig. 5. Comparison of heat propagation between two types of short: (a) the instantaneous power generated at the time of short between copper and aluminum current collectors; (b) the corresponding temperature distribution within the cell; (c and d) the corresponding profiles for the short between carbon and aluminum. The arrow marks point to the location of the short-circuit.

factor that makes the Type iii shorts the most dangerous is inadequate heat transfer on the anode side of the short (See Fig. 5). As a result of the large current flow, low reaction heats and poor heat distribution, the short-circuit between aluminum and carbon is the worst scenario of internal short within the cell.

(iv) *Cathode active material/anode short*. While this is the most probable short scenario inside a cell, given the poor conductivity of the cathode, this is also practically the most preferred case. As shown in Fig. 3, the amount of heat generated is about the same as Type ii. However, the rise in cell temperature is higher than Type ii since the thermal conductivity across the anode is lower than that across the copper current collector. The temperature rise is limited to a few degrees above the ambient temperature as observed in Fig. 4. This implies that the current typically leaks across the short.

Fig. 5 shows the instantaneous power generated for two short scenarios – between the two current collectors, and between the carbon electrode and the aluminum current collector. As seen on Fig. 5a and c, the power generated by the short between the current collectors is about three to four times higher than the Type iii short. Fig. 5b and d shows the corresponding temperature distributions for the two cases: as observed, the maximum temperature for the Type i short is significantly lower than that for the Type iii short-circuit.

3.2. Surface area of the anode and the impact of lithiation

The anode of a lithium ion cell is far more reactive when at the fully charged state, because of the presence of nascent lithium, which is highly reactive even at ambient temperatures. In addition to the high reactivity, the reactions involving lithium have very high heats of reactivity and are usually exothermic. As a result, a fully lithiated anode is several times more likely to be prone to runaway. The impact of lithiation is simulated in this model by assuming that the reactivity of lithium is directly proportional to the surface area of the carbon active material. This dependence has been observed in experiments as well [14]. Hence, for our case, the degree of reactivity of metallic lithium with the solvent and other components of the cell are measured in terms of the electrochemical surface area of the anode.

The material balance for lithium at the anode surface assumes that lithium is deposited if the potential at the interface is below the lithium deposition potential (0 V vs. Li/Li^+). The porous electrode model is solved using the parameters shown in Table 1, for two different values of the anode surface area (a_n): 0.5 and 2.0 $m^2\,g^{-1}$. If the potential at some point on the electrode surface reaches a value below 0 V, the amount of lithium metal deposited is calculated using the local flux at that point and Faraday's laws. This amount of lithium is then used as the initial value at that point in the rate equation for the reaction between lithium and other cell components. Fig. 6 shows the rise in the cell temperature for three different cases,

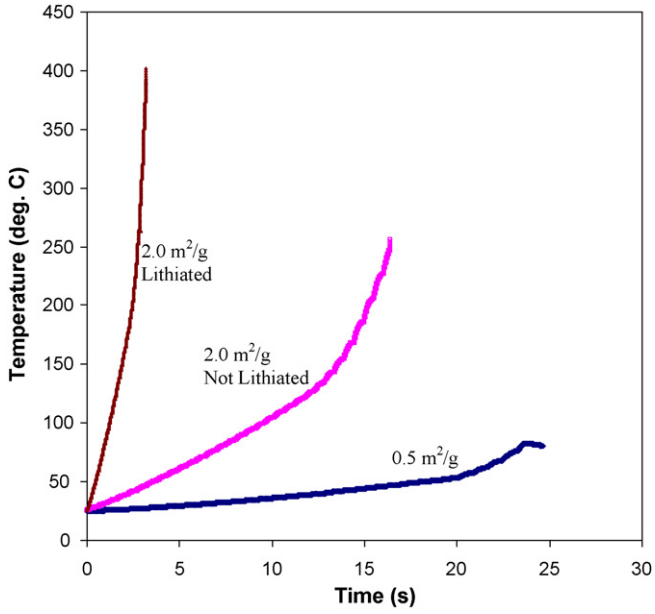

Fig. 6. Comparison of maximum temperatures as a function of surface area of carbon and the extent of lithiation during a short-circuit between the two active materials.

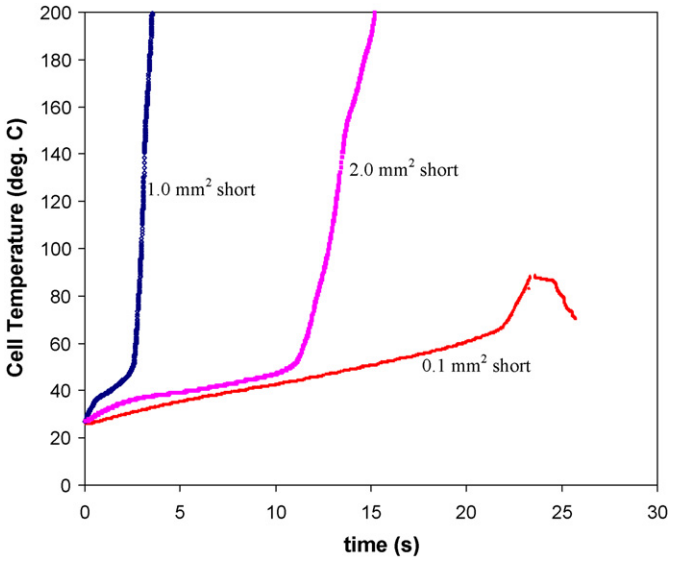

Fig. 7. Impact of short-circuit area on the temperature of the cell: (a) micro-short: the area of the short-circuit was fixed at 0.1 mm^2; (b) macro-short: short-circuit area $\leq 1\ mm^2$; (c) large macro-short: area >1 mm^2. For the set of parameters used in this model, the cell capacity is not adequate to power shorts of area >1 mm^2 with the maximum current density.

when the aluminum vs carbon short is simulated. The cells were fully charged in each case. The first case corresponds to low surface area of carbon (about 0.5 $m^2\ g^{-1}$) and the short-circuit was carried out in that part of the anode facing the current collector. In this case, the part of the anode in the immediate vicinity of the short is not subject to the intercalation reaction. The second case corresponds to 2 $m^2\ g^{-1}$ area, and again, the region in the immediate vicinity of the short does not participate in the lithium intercalation reaction for this case too: even though this part of the anode does not undergo any lithiation, the increase in the cell temperature is very rapid, because the reactivity of the anode increases exponentially with an increase in the surface area. The third case shows 2 $m^2\ g^{-1}$ surface area for the carbon electrode, now facing the cathode at the point of short. For this case, the rate of heating is enhanced further due to both an increase in the surface area and the presence of lithium. The maximum cell temperature is almost doubled from the previous case. Also, due to the rapid heat generation, there is an instantaneous onset of the runaway process for this case.

3.3. Impact of the short-circuit area

Fig. 7 shows the rise in temperature for short-circuit under different areas. In a lithium ion cell, typically micro-shorts from isolated lithium dendrites lead to burn out of the membrane in most cases. Hence such micro-shorts do not contain sufficient power for the short to propagate and the heat flow is arrested. On the other hand, if the short is persistent for sufficiently long periods of time, the amount of heat generated crosses the threshold limit and leads to the onset of the abuse reactions, which in turn generate more heat. The last case shown on Fig. 7 is that of a larger short-circuit area. If the cell capacity is not adequate to supply the power for the entire area of the short, the specific power values are lowered, resulting in a decrease of the maximum local temperature.

3.4. Impact of initial cell temperature

Fig. 8 shows the increase in the short temperature, for different initial temperatures of the cell. In general, even during the normal operation of the cell, the capacity of a cell during cycling is more at higher temperatures, due to the temperature dependence of intercalation and deintercalation rate constants, and the transport parameters. As shown in Eqs. (4) and (5), the rate constants for abuse reactions also show an Arrhenius type increase with rise in temperature. As a result, these reaction rates increase exponentially with the local temperature. Also, heat transfer to the area in the immediate vicinity of the short is difficult when the cell is already heated up to a higher temperature since the gradient in the heat flux is reduced.

As described earlier in Fig. 2, the onset of each abuse reaction occurs around a specific temperature. In a preheated cell, the margin for safety is reduced; the amount of heat generated from a Type i short described above may in this case exceed the threshold temperature for the abuse reactions at the anode, which in turn generate more heat to rise the cell temperature to higher values. In this context, it is advisable to use an adequate heat transfer mechanism that would maintain the cell temperature below the threshold

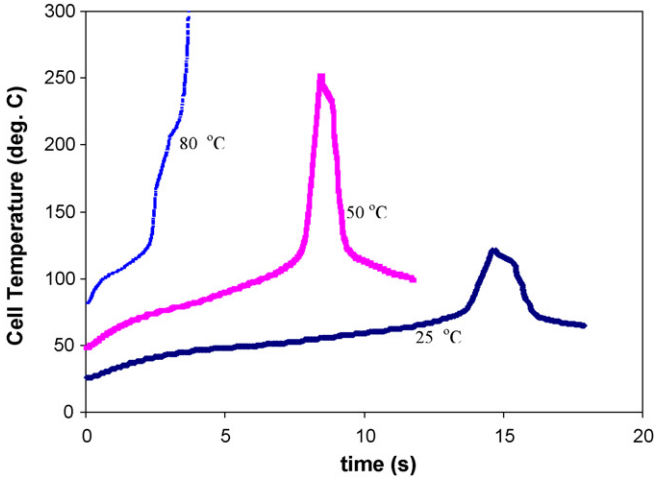

Fig. 8. Impact of initial cell temperature: three cases of short-circuit between the two current collectors of a fully charged cell are shown. Even a cell that passes the short-circuit test at room temperature has a greater tendency towards runaway for higher values of the initial cell temperature.

values for as many cases as practical. Results shown in Fig. 2 can then be used to assess the effectiveness of heat transfer from the cell.

3.5. Impact of cell capacity and SOC

Whereas both initial SOC and the cell capacity determine the local power due to current flow across the short-circuit, there are other individual effects of these parameters on the internal short behavior of a cell. The SOC for example directly relates to the extent of lithiation of the anode; and the effects of this factor were described in a previous section. As a result, under identical conditions, a cell at a lower SOC has a better chance of survival in case of an internal short. For the parameters shown in Table 1, the critical cut-off value for the SOC beyond which the runaway process sets in, is about 87%, for the Al/C case. Similarly, cell with a higher capacity implies a larger Joule (I^2R) heat up. Also, the availability of reactants for the runaway reactions is more. Fig. 9 shows a comparison of average cell temperatures during an internal short at different depths of discharge, for two cells of capacities 800 mAh (Type A) and 1800 mAh (Type B). The cell parameters were assumed to be identical except for the length of the electrodes. Two distinct observations can be made: first, the larger cell heats up faster from the instant of short, due to a higher Joule heat up; second, cells with higher states of charge progressively show an exponential rise in the rate of increment of the average cell temperature. Moreover, the higher capacity Type B cells are susceptible to runaway at values of SOC for which the Type A cells were observed to be safe.

3.6. Impact of oxygen availability

In order to simulate the effect of cell venting, the following procedure was adopted to calculate the effect of oxygen availability. The stoichiometry of the cell was used to determine the weight of the individual components (such as the solvent, binder, active material, etc.) present within the cell. The theoretical amount of oxygen required for complete combustion of each component was calculated based on the stoichiometry of the reactions. These numbers were then compared against the available oxygen within the cell, to provide estimated amounts of heat generation due to cell venting.

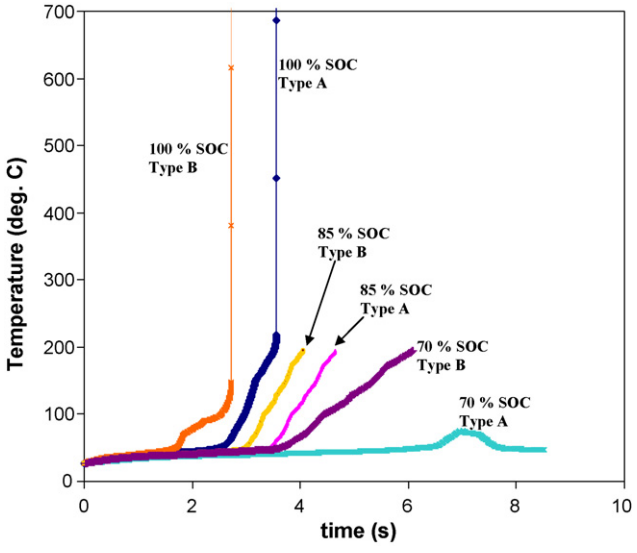

Fig. 9. Impact of SOC of the cell at the time of short on cell safety: (a) the short-circuit was assumed to occur when the cell was fully charged, (b) at the instant of short, the cell has drained 15% of its capacity; the internal short shows delayed failure, and (c) at the instant of short, the cell has drained 30% of its capacity; the internal short shows a rise in temperature, but not sufficient to trigger the runaway process. Type A cells have a capacity of 800 mAh and Type B cells have a cell capacity of 1.8 Ah.

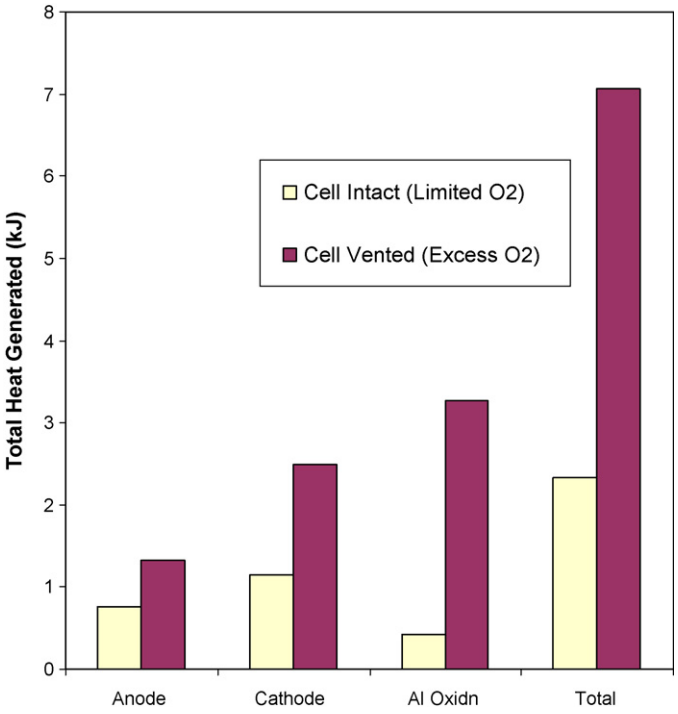

Fig. 10. Effects of excess oxygen availability: the reactions at the cathode, rapid oxidation of the current collector in particular, generate more heat when the cell vents.

Fig. 10 shows that when the cell remains intact, the combustion process is limited by the availability of oxygen to a significant extent. The oxygen released from the solvents and from the cathode material is not sufficient to generate the theoretical maximum heat, even if the maximum cell temperature exceeds the critical values reported in Fig. 10 for the onset of runaway. As a result, the venting of the cell, leading to availability of excess oxygen will at the worst cases increase the amount of heat evolved by two to three times, compared to a cell that does not vent. Whereas this aspect might not be effective in preventing the onset of the runaway reactions, appropriate design of cell container material must consider such aspects, in order to prevent rapid propagation of runaway, especially in battery packs where the heat generated from the runaway reaction in one cell influences the behavior of the other cells around. At the same time, spacing between cells in a pack must account for such worst-case scenario. Hermetic sealing of the entire pack, though it adds additional weight to the pack, may prove to be a viable alternative. Another aspect of interest in the choice of packing material is the extent of heat transfer. It was shown in an earlier section that the effectiveness of heat transfer plays a crucial role in the control of maximum cell temperature.

3.7. Experimental verification

In order to compare the model predictions with some experimental observations, internal short-circuit tests were carried out in lithium ion cells by inserting a nickel particle between different layers of the cell to create the four types of short described earlier in this paper. Prismatic lithium ion cells were fabricated using MCMB anode and cobalt-based cathode material. After formation of the first few initial cycles, the cells were disassembled in fully charged condition. The jelly roll was then unwound and a nickel particle sufficiently large to initiate an internal short was placed in appropriate regions to create the desired type of short-circuit. The jelly roll was then compressed using a flat jig at the point where the nickel particle was inserted. The cell temperature and voltage were

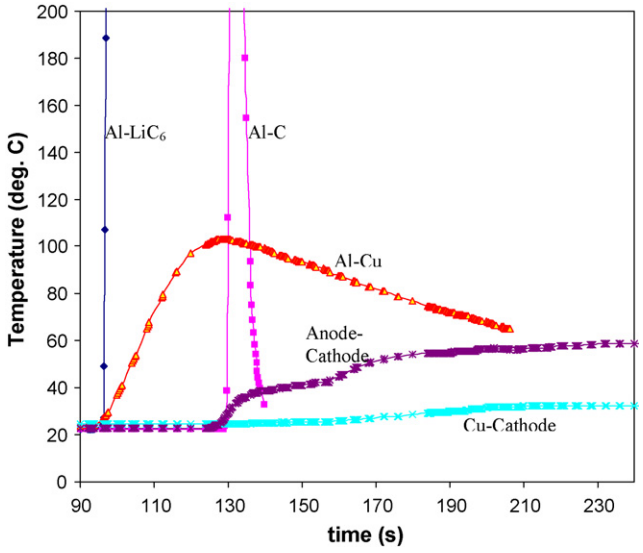

Fig. 11. Experimental measurement of cell temperature during the various types of short-circuit scenario.

monitored during the short-circuit process as a function of time. The experiment was repeated for different cases: short between the two current collectors, between the two active materials and between one current collector and the other active material. When required, part of the electrode material was scraped off to provide direct access to the current collector at the point of short-circuit. In the case of carbon vs. aluminum current collector, two different short scenarios were implemented: in the first scenario, the short was initiated between the aluminum current collector and lithiated carbon and in the second scenario; the short was initiated between aluminum current collector and the portion of anode that does not take part in the intercalation process. In all these cases, the cells were fully charged before disassembly and subjected to the short-circuit studies.

Fig. 11 shows that the experimental curves show the same qualitative trend as predicted by the model under identical conditions. It is worth mentioning that the process of internal short-circuit is almost instantaneous and governed by the behavior of the reactants at the local spot of initiation of the short. Hence attaching quantitative significance to such results is not encouraged. In other words, whereas the results shown here are qualitatively typical of the respective scenarios, the actual numeric values for the maximum temperature of the cell or the instant of short-circuit is not reproducible from one trial to another. Similarly, upon suitable choice of materials and alternate cell designs, the behavior of the cell can be altered. Nevertheless, the experimental results described in this work provide an insight into the conditions that are most probable candidates for thermal runaway in the event of an internal short-circuit.

4. Conclusions

A systematic study of the internal short-circuit mechanism inside a lithium ion cell was carried out. Several short-circuit scenarios were simulated using a thermal-electrochemical abuse model and the results were verified with some experimental studies. The short between the lithiated anode material and the aluminum current collector was found to result in maximum heat generation. In almost all scenarios, the origin of the trouble during runaway is from the anode; as a result, safer design of anodes provides for better chances of surviving an internal short. The fully charged cells generate more heat owing to the greater potential difference between the electrodes. Cells of larger capacity drain more current and thus lead to higher heat generation rates. Use of forced convection is recommended to keep the maximum temperature of the cell low, and thus increase the chances of the cell passing a safety test. Most cells have limited oxygen availability and hence safety during an abuse scenario can be enhanced by appropriate design of the packaging material. Safe design of a cell can be achieved using the approach presented here: the actual implementation requires an extensive measurement of the material properties under a variety of abuse conditions. Such an investigation, though exhaustive, will provide definitive answers for today's challenges posed by the safety requirements.

Acknowledgements

The authors would like to acknowledge the help from colleagues and staff members at Celgard. This work was supported by Celgard LLC.

References

[1] R. Spotnitz, J. Franklin, J. Power Sources 113 (2003) 81–100.
[2] T.D. Hatchard, D.D. MacNeil, A. Basu, J.R. Dahn, J. Electrochem. Soc. 148 (2001) A755–A761.
[3] G.G. Botte, R.E. White, Z. Zhang, J. Power Sources 97–98 (2001) 570–575.
[4] K. Onda, H. Kameyama, T. Hanamoto, K. Ito, J. Electrochem. Soc. 150 (2003) A285–A291.
[5] E.P. Roth, D.H. Doughty, J. Power Sources 128 (2004) 308–318.
[6] T. Yamauchi, K. Mizushima, Y. Satoh, S. Yamada, J. Power Sources 136 (2004) 99–107.
[7] G.-H. Kim, A. Pesaran, R. Spotnitz, J. Power Sources 170 (2007) 476–489.
[8] R.M. Spotnitz, J. Weaver, G. Yeduvaka, D.H. Doughty, E.P. Roth, J. Power Sources 163 (2007) 1080–1086.
[9] D.P. Abraham, E.P. Roth, R. Kostecki, K. McCarthy, S. MacLaren, D.H. Doughty, J. Power Sources 161 (2006) 648–657.
[10] Barnett et al., Presentation at 24th International Battery Seminar & Exhibit, Fort Lauderdale, Florida, 2007.
[11] J.S. Newman, Electrochemical Systems, 2nd ed., Prentice-Hall, Englewood Cliffs, NJ, 1991.
[12] J.S. Newman, K.E. Thomas, H. Hafezi, D.R. Wheeler, J. Power Sources 119–121 (2003) 838–843.
[13] W.B. Gu, C.Y. Wang, Electrochemical Society Proceedings 99–125 (1) (2000) 748–762.
[14] D.D. MacNeil, D. Larcher, J.R. Dahn, J. Electrochem. Soc. 146 (1999) 3596–3602.
[15] W.B. Gu, C.Y. Wang, J. Electrochem. Soc. 147 (8) (2000) 2910–2922.